



Article

Mineralogical, Petrological and Geochemical Characterisation of Chrysotile, Amosite and Crocidolite Asbestos Mine Waste from Southern Africa in Context of Risk Assessment and Rehabilitation

Jessica Shaye Schapira ^{1,2,*} , Robert Bolhar ¹, Sharad Master ² and Allan H. Wilson ¹ 

¹ School of Geosciences, University of the Witwatersrand, Johannesburg 2050, South Africa; robert.bolhar@wits.ac.za (R.B.); allan.wilson@wits.ac.za (A.H.W.)

² School of Molecular and Cell Biology, University of the Witwatersrand, Johannesburg 2000, South Africa; sharad.master@wits.ac.za

* Correspondence: jessschapira@gmail.com

Abstract: Derelict asbestos mine sites in South Africa pose a considerable risk to human, environmental and socio-economic health. Comprehensive mineralogical and geochemical datasets for the existing hazardous geological materials still exposed in Southern African derelict asbestos mines remain largely non-existent, as very little published and up-to-date literature is available. In this study, three representative types of asbestos mineral fibres from derelict asbestos mines in Southern Africa, namely chrysotile from Havelock mine, amosite from Penge mine and crocidolite from Prieska mine, are characterized mineralogically and geochemically to critically evaluate actual hazards in rural and asbestos-fibre-contaminated regions. The samples were examined using polarising light microscopy, X-ray fluorescence (major and trace elemental analysis), X-ray diffraction (including Rietveld refinement), specific surface area analysis and bio-durability testing. Data are discussed in view of their potential toxicities on both human health and the environment in the context of developing countries. Finally, information on the mineralogical and geochemical status of asbestos mine waste and its importance as baseline data for rehabilitation considerations is also evaluated.

Keywords: hazards; rehabilitation; dispersion; environmental; mine waste



Citation: Schapira, J.S.; Bolhar, R.; Master, S.; Wilson, A.H. Mineralogical, Petrological and Geochemical Characterisation of Chrysotile, Amosite and Crocidolite Asbestos Mine Waste from Southern Africa in Context of Risk Assessment and Rehabilitation. *Minerals* **2023**, *13*, 1352. <https://doi.org/10.3390/min13101352>

Academic Editors: María de la Luz García Lorenzo, José María Esbrí and Oscar Andreu Sánchez

Received: 2 October 2023

Revised: 15 October 2023

Accepted: 16 October 2023

Published: 23 October 2023



Copyright: © 2023 by the authors. Licensee MDPI, Basel, Switzerland. This article is an open access article distributed under the terms and conditions of the Creative Commons Attribution (CC BY) license (<https://creativecommons.org/licenses/by/4.0/>).

1. Introduction

The mineral wealth of South Africa is impressive but matched perhaps only by the subsequent environmental and human health problems resulting from mining. There are ~6000 derelict mines throughout South Africa, which pose significant health and environmental concerns [1]. Of these, 249 are abandoned asbestos mines of which less than 40 have been rehabilitated [1]. A legacy of pollution remains in the wake of the asbestos mining industry, and considerable quantities of rock-waste generated by decades of asbestos mining continue to pose an insurmountable health and environmental risk to surrounding communities, especially those in developing countries [2]. Historically, poorly regulated asbestos mining operations in South Africa have resulted in the widespread contamination of the environment. Although occupational exposures diminished in the wake of the asbestos mining cessation in South Africa, the tenacious, contemporary, and vast asbestos contamination of the environment is indicative of an indeterminate and conceivably boundless epidemic of asbestos-related diseases (ARDs) [3].

The regulatory and commercial term, asbestos, defines a group of naturally occurring silicate minerals with a specific fibrous crystal habit and unique chemical, physical and technological properties [4]. There are six types of asbestos minerals that fall into one of two groups, namely serpentine and amphiboles [5]. Repeated experimentations have strongly proven the association between asbestos exposure and cancer types such as carcinoma [6–8].

The toxicity and carcinogenic effects of asbestos-mineral fibres are related to the physical and chemical properties, including morphology, durability and/or bio-persistence, high aspect ratio and chemical composition of these fibrous minerals [9–13]. The airborne dispersion of asbestos fibres through human activities and rock weathering increases the potential for inhalation of fibres, resulting in risks to human health [14–19]. Asbestos minerals also have a high capability to host a vast quantity of toxic species and elements, adding to the potential health risk problem [18,19]. Asbestos-related diseases (ARDs) acquired from environmental sources are undeniably a global concern [3,20]. Numerous types of asbestos-related diseases include both diseases of the pleura and diseases of the lung parenchyma [3]. Malignant mesothelioma, thickening and pleural plaques comprise the pleura diseases category, and asbestosis and lung cancer comprise the lung parenchyma diseases category [3,21]. The global scientific community, to date, agrees that, based on scientific evidence, there is no safe level or threshold of asbestos fibre exposure below which the risk of mesothelioma is negligible [22,23]. Different fibrous minerals display different toxicities due to their different physical and chemical properties [24,25].

Geochemical and mineralogical characterisation of asbestos-bearing mine rocks is important for both human and environmental health risk assessment and quantification, necessary for effective risk mitigation intervention [26]. Moreso, baseline geochemical and mineralogical data on asbestos fibre waste dumps are critical for directing rehabilitation interventions [26]. However, the costs involved in these assessments are a major issue for developing countries. The aim of this paper is to use traditional mineralogical, petrographic and geochemical methods conventionally applied to the characterisation of fibrous minerals, to demonstrate the importance of incorporating geologic-based delineation in derelict asbestos mine site rehabilitation programmes. The paper further highlights the necessity of basic geological knowledge in the context of asbestos mine reclamation and demonstrates the feasibility of relevant scientific methods that are also cost-effective, relatively rapid and easily accessible in fund-limited, developing countries.

2. Materials and Methods

2.1. Sampling Locations and Geological Background

Three different asbestos rock samples were investigated in this study (Table 1), namely (i) Chrysotile from Bulembu (Havelock Mine), Eswatini, Southern Africa (Figure 1A); (ii) amosite from Penge, Lydenberg district, South Africa (Figure 1B); and (iii) crocidolite from Prieska Division, Northern Cape, South Africa (Figure 1C).

Table 1. Location coordinates and description of sampling locations.

	Chrysotile	Amosite	Crocidolite
Sample number	Ch1	Am2	Cr3
Sampling locations	Havelock Mine, Bulembu, Swaziland (Eswatini)	Penge, Sekhukhune District, Limpopo, South Africa	Prieska Division, Northern Cape, South Africa
Location coordinates	25°57'21" S 31°07'51" E	24°25'07" S 30°20'14" E	28°19'01" S 23°06'05" E
Occurrence	Cross-vein fibres (growth of fibres at right angles to the walls of cracks)	Cross-fibre seams in banded ironstones	Cross-fibre seams in banded ironstones
Number of samples collected	Three	Two	Two

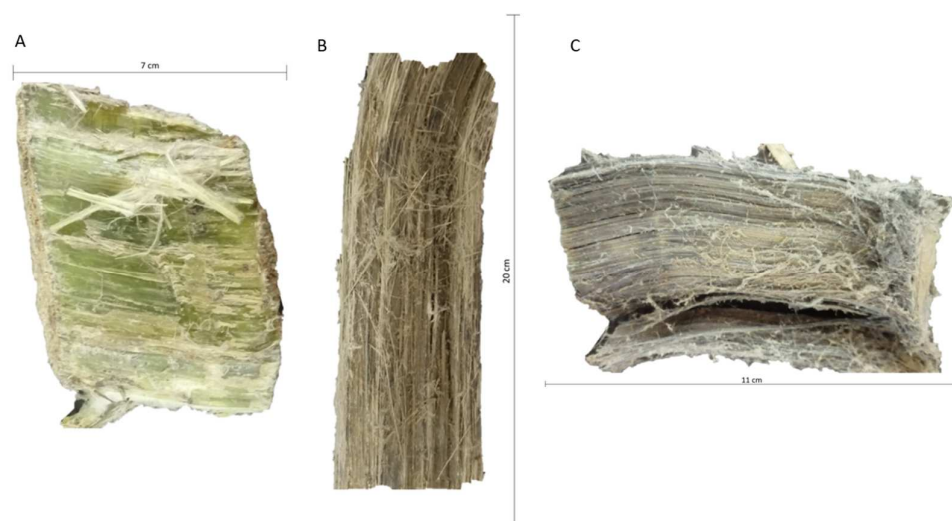


Figure 1. (A) chrysotile, (B) amosite and (C) crocidolite.

The chrysotile samples (Ch1) were collected from the Havelock mine, Eswatini. In southern Africa, the Havelock orebody is one of the largest chrysotile asbestos deposits [27]. The Havelock asbestos deposits occur within the Swartkoppie Formation of the Onverwacht Group in the south-eastern part of Precambrian layered ultramafic complexes of the Barberton greenstone belt [28,29]. Chrysotile asbestos occurs as serpentinite lenses or pods within the main lithological components of the Swartkoppie Formation [30]. The differentiated and serpentinitised ultramafic bodies contain units of pyroxenite, metagabbro, dunite and peridotite, where relict and strongly altered olivine, clinopyroxene, orthopyroxene and chromite are the major rock forming minerals [31]. The asbestos deposits are structurally controlled and localised within the deformation zones of the host rocks in the form of cross-fibres in a stockwork of veins [27,30,32]. Hydration resulted in the partial or complete serpentinization of the ultramafic rock [31]. Chrysotile asbestos formation requires a specific combination of tectonic controls including folding, faulting, shearing, serpentinization and metamorphism [31]. The original material is provided by the host rocks to form veins and therefore fibre composition reflects vein composition [33].

The amosite samples (Am2) were collected from Penge, Limpopo Province where they occur as layered, extensive continuous seams within the banded iron formations (BIF) [34]. Situated in the metamorphic aureole of South Africa's Bushveld Complex, the Penge Iron Formation of the Transvaal Supergroup is a unique succession as it contains both amosite and crocidolite asbestos [35,36]. The distribution of amosite and crocidolite asbestos seams in the Penge Iron Formation are controlled by bulk-rock composition. However, some evidence suggests that with increasing metamorphic grades, amosite replaced crocidolite [36]. The fibrous amosite units in the BIF are in transitional contact with and underlain by a thick dolomitic sequence [31]. An angular unconformity marks the upper contact of the BIF, which is overlain by a quartzites and shale sequence. Alternating bands of dark-coloured magnetite, grunerite and graphite and light-coloured chert, quartz and siderite comprise the iron formation [36]. The bands are laterally extensive and range from several centimetres in thickness to microscopic [37]. The fibrous amosite asbestos is found as clearly defined lithological units [36], typically in several units of micro-banded magnetite-grunerite banded iron formation [36]. For the most part, amosite is found in lenses of fibrous masses with their long axes perpendicular to the country rock [38].

The crocidolite samples (Cr3) collected from the Prieska Mine in the Northern Cape occur as seams interbedded within the banded iron formations [34]. In the Northern Cape the crocidolite fields extend >450 km south of Prieska to the border of Botswana, where the blue fibres occur in the Asbestos Hills BIF as 1 to 50 mm cross-fibre seams [32,39].

Lengths of fibres are important when considering their removal from the lungs via macrophage cells that under normal circumstances eliminate foreign particles from the

lungs [40]. Fibres with lengths greater than the diameter of macrophages cannot be removed, resulting in macrophage death and inflammatory cytokines release into surrounding tissues resulting in fibrosis or asbestosis if inhaled as collagen builds up [41]. Numerous studies have indicated that fibres with lengths less than 5 μm do not have any significant biological potency as they are cleared by macrophages [42]. Fibres with lengths > 10 to 15 μm have a greater probability of persisting in the lungs for extended time periods [42]. Thus, length characterisation of exposed asbestos-containing mine rock waste is important with regard to the relative health risks and effects [40].

Crocidolite is believed to have formed mainly from sodium-rich brines that moved through the iron formation [37]. Unlike the host rocks, crocidolite is extremely resistant to weathering and persists at the surface [31]. The fibrous crocidolite asbestos deposits demonstrate significant blue colour variation [31].

2.2. Polarised Light Microscopy (PLM)

Visible asbestos fibers extracted from their host rocks were cut with scissors and positioned on a glass slide. A small drop of eugenol (refractive oil index $n = 1.54$) was then deposited on the fibres after which they are covered with cover slips. The slide was optically scanned, and the asbestos mineral was identified using its optical properties (morphology, colour, pleochroism, birefringence, extinction characteristics and sign of elongation). Coatings on the fibres sometimes obscure the optical properties of the asbestos minerals and fibres finer than the microscopes resolving power (ca. 0.3 μm) and are not detectable. The asbestos mineral fibres colour and index of refraction may be altered or changed by acid and heat treatment.

2.3. Crushing

Simple crushing, using a mortar and pestle, enabled to explore whether the long, visibly elongated minerals in each of the rock samples are fibrous. Elongated minerals sometimes become matted together during crushing and form a ball and/or separate into needles or fibres; these are considered as fibrous and potentially asbestiform. Those that are easily crushed into a powder are not fibrous and therefore deduced not to be asbestiform. However, cleavage fragments and asbestiform fibres may occur in close association. Powdered samples were studied using X-ray diffraction (XRD), X-ray fluorescence (XRF) and Brunauer–Emmett–Teller (BET) surface area analysis. A rotary splitter was used to reduce the samples, which were then powdered in a mortar and pestle.

2.4. X-ray Diffraction (XRD)

The samples were analysed via X-ray diffraction (XRD) to determine the mineral type. The XRD analysis was performed by using the back-loading preparation method. Diffractograms were attained by employing a Malvern Panalytical Aeris diffractometer with PIXcel detector and fixed slits with Fe filtered $\text{Co-K}\alpha$ radiation. Phases were determined by means of X'Pert Highscore plus software (version 2.1. PANalytical, Malvern, UK). The Rietveld method (quantitative analysis) [43] was used to estimate the relative phase amounts (weight %). The phases were identified using X'Pert Highscore plus software. The relative intensities and d -spacing were calculated from the diffractogram data.

2.5. X-ray Fluorescence (XRF)

Major and trace element concentrations of the four asbestos mineral fibre samples were determined using X-ray fluorescence (PANalytical PW2404 x-ray spectrometer). Major elements were determined using the Norrish Fusion 1 technique [44] using in-house correction procedures outlined in [45]. Sample weight used was 0.35 gm and flux weight of 2.5 gm. Samples were fused using Johnson Matthey Spectroflux 105 at 1100 $^{\circ}\text{C}$ and raw data corrected. Standard calibrations were prepared using synthetic oxide mixtures, international standard as well as in-house controls. Calibration standards were from International Reference Materials USGS series (USA) and NIM series (South Africa). Pressed

pellets were prepared for trace element analysis and the data corrected for matrix effects using Compton peak monitoring.

2.6. BET-N₂ Specific Surface Area Determination

Specific surface area is an important characteristic of mineral fibres [46] and a significant parameter related to the many attributes linked to its toxicity and carcinogenicity [47,48]. The specific surface area of the asbestos rock samples was determined via the BET method [49] using a Micromeritics TriStar 3000 V6.05 A surface area analyser with N₂ as absorbing gas. A mass of ~0.2 g of each sample was placed in BET sample tubes and degassed for 4 h. The samples were then loaded into the BET instrument and N₂ adsorption isotherms were obtained to determine the specific surface area.

2.7. Bio-Durability Tests

The ability of mineral fibres to resist chemical and/or biochemical alteration is referred to as biodurability [50–52]. The biodurability of the asbestos samples was determined through batch dissolution experiments at 37 °C and continuous agitation (90 rpm). Batch dissolution experiments (water–rock interaction study) allow for dissolution rates to be measured in a setting dominated by fluids [53,54]. The experiments were conducted at 37 °C to simulate body temperature [53]. Although the intricacy of the human body cannot be replicated, these experiments provide a basis to assess the biological disintegration of the different mineralogical types of asbestos [53]. Seven batch reactors were set up for each type of asbestos sample and the change in sample mass at different intervals of time was measured. The advancement of the dissolution reaction was determined at the following sampling times: 24 h, 48 h, 1 week, 2 weeks, 1 month, 2 months and 3 months. The batch experiments were conducted in 100 mL Erlenmeyer flasks containing water and HCl solution (50 mL) at a pH of 4 and 50 mg of sample. At each sampling time, the content of the flask was vacuum filtered using 0.22 µm φ (phi) cellulose Merck Millipore filters (ashless grade). The mass of the solid residue was determined by measuring the weight difference of the initial sample mass and the solid residues, after filtration and drying, known as the filter mass. The following equation was used to calculate the dissolved mass fraction (DMF) of the chrysotile, amosite and crocidolite (Equation (1)):

$$\text{DMF} = 1 - \frac{M_t}{M_o} \text{ or } \text{DMF} = \frac{M_o - M_t}{M_o} \quad (1)$$

where M_o is the initial mass of the solid at time = 0 and M_t is the mass of the solid at time t .

The dissolution efficiency of the chrysotile, amosite and crocidolite was also calculated using the raw data of total mass loss after 720 h. The dissolution efficiency (D%) of the asbestos rock sample in HCl-water solution was calculated according to Equation (2) [55,56]:

$$\text{D}\% = \frac{M_i - M_t}{M_i} * 100 \quad (2)$$

where M_i is the initial mass (grams), and M_t is the total mass loss (g).

3. Results

3.1. Bulk Material Description

Chrysotile (Ch1) collected from the Havelock Asbestos Mine (Bulembu) appears homogeneously distributed within the rock (Figure S1A). These chrysotile fibres occur in veins in the serpentinite (Figure S1B). The fibres within the veins display a combination of straight, curved, and contorted forms. A partitioning parallel to the vein walls caused splitting of the cross-fibre vein and subsequent shortening of the fibre length in relation to the vein width (Figure S1D). Such disassociation affects the degree of fibre to sidewall cohesion enabling fibres to separate easily and become dispersed from the host rock. The highly fibrous components occupy ~80% of the rock sample and are easily separable. The bundles of chrysotile fibres are pale green in colour but separate to form a fluffy mass

of white fibres (Figure S1C). The individual fibres are extremely fine, flexible and have a curved and wavy appearance. When observed individually, the chrysotile fibres are white in colour and have a silky lustre. The crystals comprising the fibres are short (~2.5 cm) and extremely hair-like. The mineral fibres retained their fibrous form and aspect ratio upon crushing in a mortar and pestle. The fibres can be bent and twisted without breaking indicating that the chrysotile fibres have high tensile strength.

The amosite (Am2) consists of long (~20 cm), thin, straight, brown coloured fibres that form in bundles and have a ‘paintbrush-end’ effect (Figure S2A). The fibres from the amosite sample are very brittle and ‘shatter’ easily when brushed with the dissecting forceps. The bundle of amosite fibres demonstrates a slight curvature because of their long length. The surface of the amosite fibre bundle shows individual matted and splintery fibres (Figure S2B).

The crocidolite sample (Cr3) consists of long (~10 cm), straight, greyish to pale blue coloured fibres in a bundle (Figure S3A). The poly-filamentous bundle is macroscopically curved and contorted (Figure S3B) indicating flexibility. The fibres are brittle and have a silky lustre. The bundle of fibres is easily parted, with a longitudinal fine structure, and is tufted at the ends. These fibres show partial flexibility when bent.

The elongated shape of the minerals visibly observed in hand sample allowed direct length measurements to be taken (Table 2).

Table 2. Fibre lengths for 21 counts for each mineral in hand sample.

Counts	Chrysotile		Amosite		Crocidolite	
	Length (cm)	Width (µm)	Length (cm)	Width (µm)	Length (cm)	Width (µm)
1	2.5	12.5	20	28.5	6	6.25
2	0.5	12	5	26.5	10	6.2
3	1.2	12.2	15	28	11	6.3
4	1.8	12.2	10	23.8	8	6
5	2.2	12.6	9	25.5	8	6
6	0.9	12.1	13	28	6	6
7	1.36	12.3	19	25	10	6.2
8	2.4	12.3	7	26.5	10	6.2
9	2.5	12.4	18	28	9	6.2
10	1.9	12.5	18	22.3	6	6.2
11	1.7	12	16	20.5	6	6.3
12	2.1	12.1	15	28.1	8	6
13	0.8	12.4	13	28.2	9	6.1
14	2	12.6	8	28	10	6
15	2	12.4	15	20.2	10	6.2
16	1.1	12.3	5	17	10	6.2
17	0.6	12.2	8	20	6	6.2
18	2.5	12.2	11	18.9	8	6.3
19	2.3	12.2	19	20	10	6.1
20	1.7	12.2	20	28.5	6	6.2
21	2	12.6	20	27.1	6	6.2
Average	1.72	12.3	13.52	24.7	8.24	6.16
Minimum	0.5	12	5	17	6	6
Maximum	2.5	12.6	20	28.57	11	6.3
Variance	0.40	0.30	25.11	13.87	3.13	0.01
Standard dev.	0.63	0.18	5.01	3.72	1.77	0.10

3.2. Polarised Light Microscopy (PLM)

The cross-polarizing light microscopy images of chrysotile, amosite and crocidolite are shown in Figure 2.

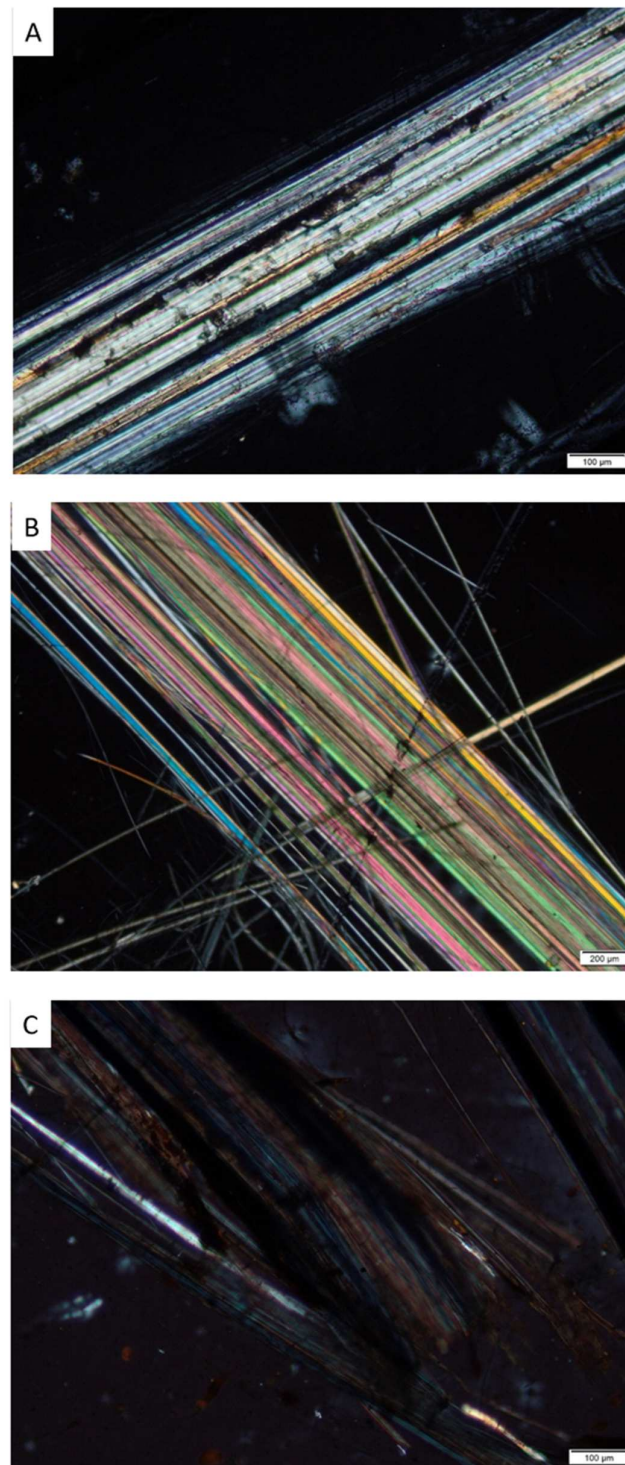


Figure 2. (A) Sample Ch1. Partially altered chrysotile fibres shown by amorphous, irregular material and cloudiness (XPL); (B) Sample Am2. Extremely fine amosite fibres showing parallel alignment and matting (XPL), and (C) Sample Cr3. Crocidolite fibres with splayed ends (XPL).

The morphology of the chrysotile fibres is asbestiform containing kinks and larger bundles with splayed ends. In plane polarised light (PPL), the chrysotile fibres have

low relief and show weak pleochroism with purple, light, and dark brown and pale-yellow colours observed (Figure S4). In cross polarised light (XPL), the fibres give off pale interference colours, including white, yellow, orange, red and purple and show a parallel extinction angle (Figure S5). The individual fibres are distinct in both PPL and XPL by various colours and birefringence. The cloudy yellow-orange character of certain bands in XPL emphasises the structure of these veins. The margins of the fibres are outlined with serpentine or material shown as irregular, slightly anisotropic and potentially cryptocrystalline (Figures S6 and S7).

The morphology of the amosite fibres is asbestiform with straight fibres and fibre bundles. The ends of the fibre bundles show a broom-like or splayed appearance. Under plane polarised light (PPL), the amosite has a weak to medium relief and weak to moderate pleochroism displaying brown, purple, pale-green, and pale-yellow colours. In cross polarised light (XPL), pink, blue, purple, yellow, orange, and white interference colours are observed along with a parallel extinction angle. Extremely fine amosite fibres with parallel alignment and matting are shown in Figures S8 and S9. The maximum angle of pleochroism and birefringence is observed at 45° (Figures S10 and S11).

The morphology of the crocidolite fibres is asbestiform with straight fibres and fibre bundles. In plane polarised light (PPL), the crocidolite fibres have moderate relief and are weakly pleochroic with blue, black, and pale-yellow colours displayed (Figure S12). Under cross polarised light (XPL), blue and pale-yellow interference colours and a parallel extinction angle are observed (Figure S13). The fibre bundles have clearly observed splayed ends (Figures S14 and S15). Crocidolite shows the least number of interference colours amongst all three of the various asbestos mineral fibres studied.

3.3. X-ray Diffraction (XRD)

Although the fibres were individually extracted and clearly identifiable impurities removed, some mineralogical heterogeneity is unavoidable, and thus, XRD was employed to determine the bulk mineralogical compositions of the asbestos samples and the recognition and identification of any impurities in each sample. The XRD diffraction patterns (λ (CoK α) = 1.78892) of the samples are shown in Figure 3 with the corresponding numerical 2θ position and intensity data given in Table S1.

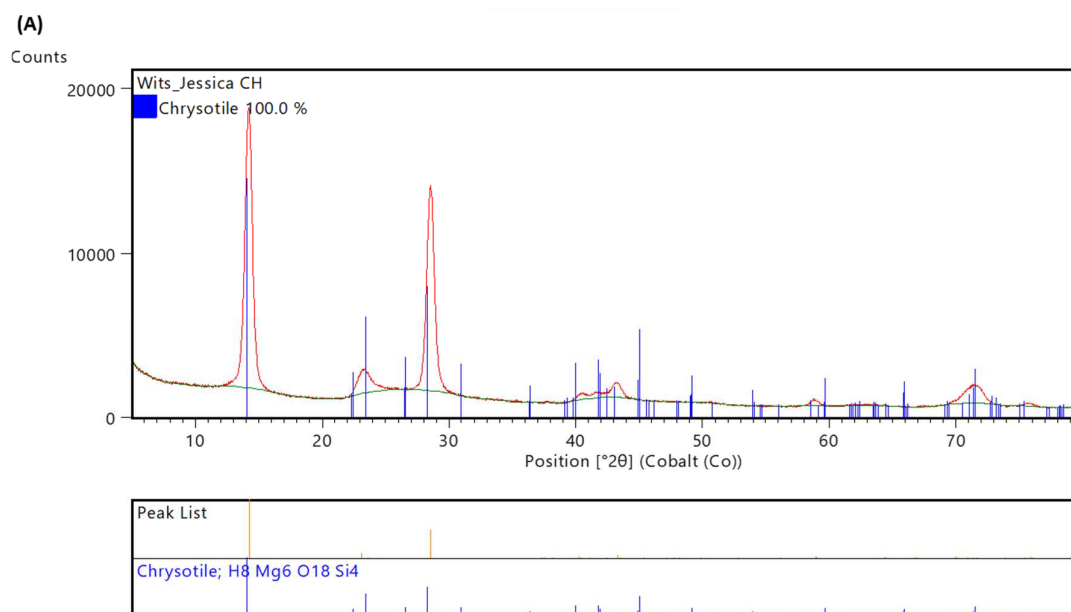


Figure 3. Cont.

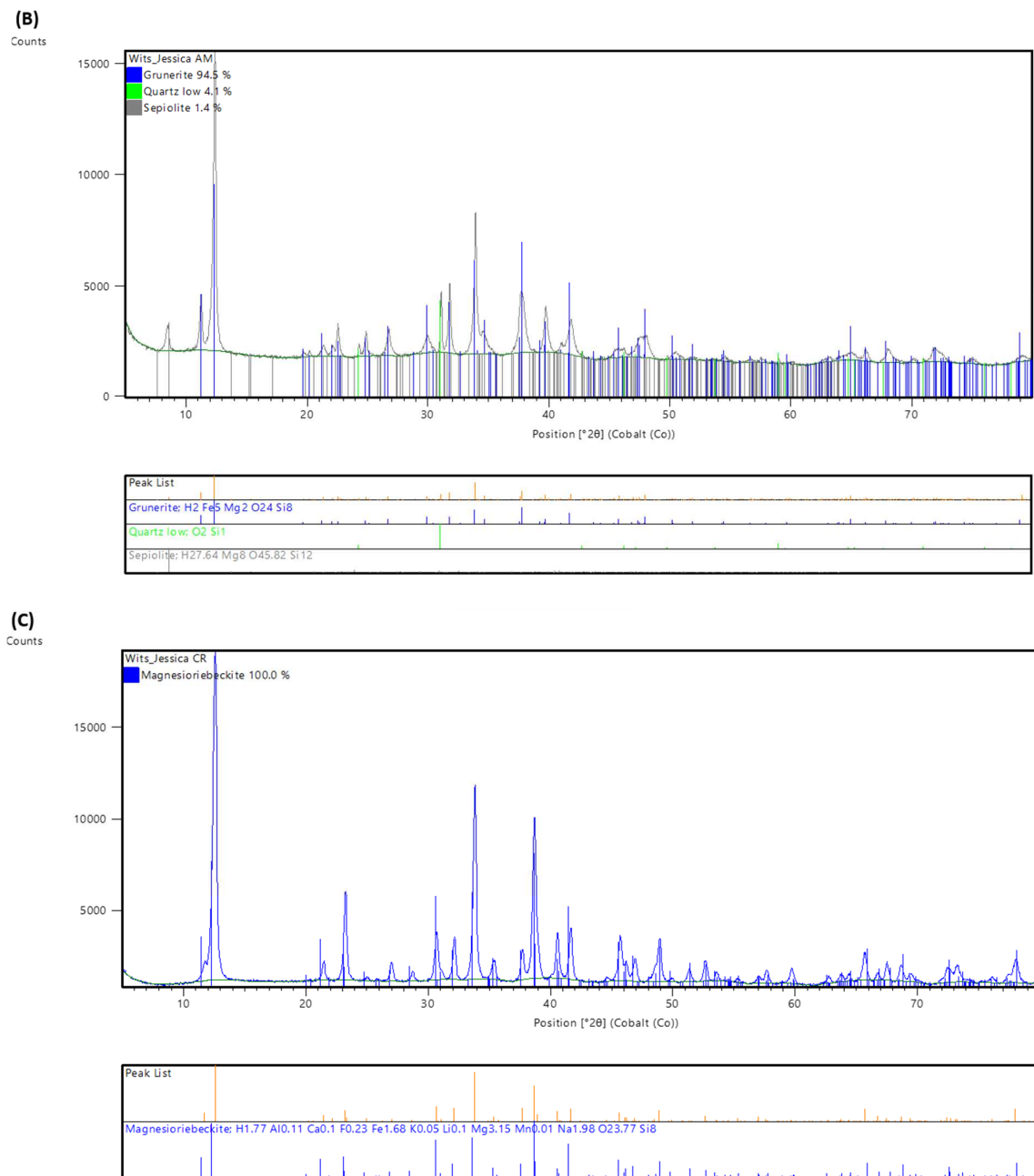


Figure 3. (A) Sample Ch1. Chrysotile asbestos XRD diffractogram and Rietveld refinement phases; (B) Sample Am2. Amosite asbestos XRD diffractogram and Rietveld refinement phases; and (C) Sample Cr3. Crocidolite asbestos XRD diffractogram and Rietveld refinement phases.

The relative intensity and d -spacing calculated for the chrysotile, amosite (grunerite) and crocidolite (magnesio-riebeckite) phases (Table S1) correspond to those of the known principal lattice spacings for each of the asbestiform minerals [57]. The Rietveld refinement data are shown in Table 3.

Table 3. Abundance (%) of mineral phases detected via XRD analysis.

Asbestos Rock Sample	Phases Detected (% Composition)
Chrysotile	Chrysotile (100%)
Amosite	Amosite (94.5%) >> Quarts low (4.1%) > Sepiolite (1.4%)
Crocidolite	Magnesio-riebeckite (100%)

% abundance represents the modal amounts of minerals (quantitative analysis) present in asbestos rock samples.

Chrysotile and crocidolite can be shown to be the only mineral phases indicating the purity of the fibres in each sample. In contrast, the amosite sample contains quartz and sepiolite as two other mineral phase.

3.4. X-ray Fluorescence (XRF) Major and Trace Elemental Analysis

X-Ray fluorescens spectroscopy (XRF) was used to quantify the major and trace elements in asbestos-containing mine waste rocks. The major and trace concentrations were determined to define the amount of harmful elements that can potentially be released into both the environment and possibly absorbed by the human body. Average major and trace elemental concentrations ($n = 2$) of each asbestos rock waste are presented below (Tables 4 and 5).

Table 4. Major element analysis ($n = 2$).

Oxides (wt%)	Chrysotile	Amosite	Crocidolite
SiO ₂	42.08	48.93	51.52
Al ₂ O ₃	0.59	0.36	0.07
Fe ₂ O ₃	2.00	41.37	38.31
MnO	0.03	0.64	0.06
MgO	40.83	5.84	2.23
CaO	0.06	2.02	0.35
Na ₂ O	0.07	0.00	6.22
K ₂ O	0.01	0.24	0.10
TiO ₂	0.03	0.03	0.03
P ₂ O ₅	0.01	0.02	0.01
Cr ₂ O ₃	0.01	0.02	0.01
NiO	0.19	0.01	0.01
LOI	12.18	0.48	1.24
Total	100.08	99.87	100.15

The samples display the following distinctive major element geochemical characteristics: Chrysotile samples contain the most aluminium and magnesium; amosite samples displayed the highest concentrations of iron and calcium, and crocidolite samples contained the greatest sodium.

Table 5. Trace element analysis ($n = 2$).

Element (ppm)	Chrysotile	Amosite	Crocidolite
Sc	6.4	4.64	D.L.*
V	16.42	3.51	3.91
Cr	83.4	4.61	D.L.*
Co	52.55	D.L.*	D.L.*
Ni	1518.54	51.24	11.86
Cu	21.99	36.77	35
Zn	16.19	41.62	12.66
Ga	D.L.*	D.L.*	1.63
Rb	D.L.*	20.77	1.02
Sr	0.74	26.63	0.86
Y	0.77	3.78	1.82
Zr	0.49	3.7	0.38
Nb	D.L.*	0.85	D.L.*
Mo	D.L.*	0.62	D.L.*
Ba	D.L.*	28.17	1.69
Pb	6.62	5.32	5.06
Th	D.L.*	D.L.*	D.L.*
U	D.L.*	D.L.*	D.L.*

* D.L.—detection limit.

3.5. BET-N₂ Specific Surface Area

The specific surface area (SSA), determined by the N₂ BET procedure, of fibrous minerals is defined as the surface area per unit volume. ‘Specific’ or ‘reactive’ are two ways in which the surface area may be defined [58]. Gas adsorption and the Brunauer–Emmett–Teller (BET) equation is used to determine the specific surface area, whereby the total surface area is divided by the mass of the sample [49]. The BET N₂ specific surface areas and associated parameters of the extracted fibres are given in Table S3.

3.6. Bio-Durability Tests

The solid asbestos residue was separated from the solution via filtration at the end of each time during the bio-durability test and the mass measured (Table 6).

Table 6. Measured mass (mg) of the solid asbestos sample residue after each time period during dissolution in acidic solution.

Time (Hours)	Chrysotile	Amosite	Crocidolite
0	50	50	50
24	25.2	39.1	37.7
48	24	38.6	33.6
168	21	36.3	32.3
334	18.6	35.5	31.7
720	16.6	35.4	31.1
Total mass loss (mg)	33.4	14.6	18.9

The weight loss for all three types of asbestos reached a plateau after 186 h indicating the completion of the chemical reaction. The mass loss of the experiments for each asbestos

sample was summed up, although 100% solid mass loss is never achieved. The reason is not incomplete dissolution, but rather the precipitation of silica back out of the solution [23]. The dissolved mass fraction (DMF) calculated for the asbestos samples are given in Table S3 and graphically represented in Figure 4.

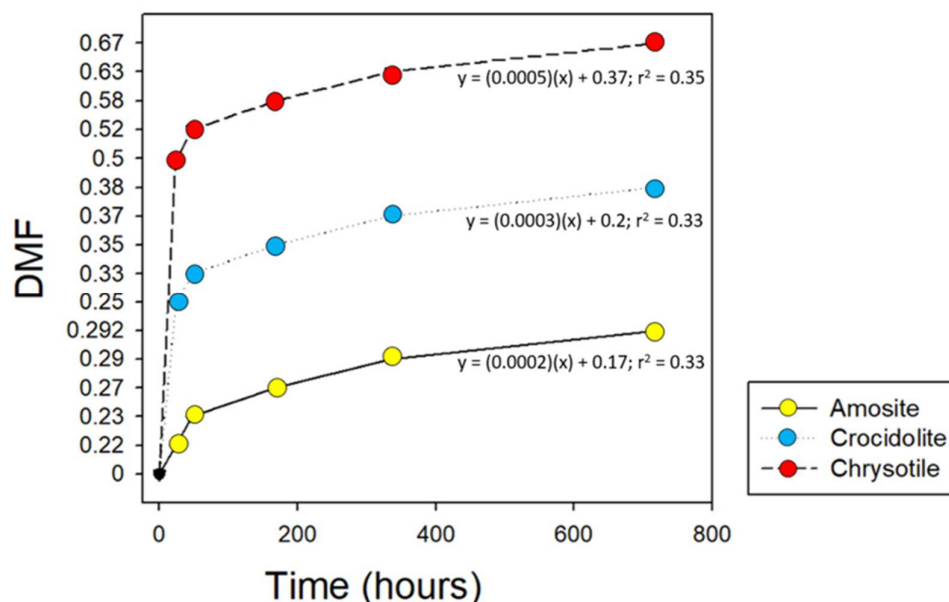


Figure 4. The dissolved mass fraction of the asbestos samples over time (hours).

The dissolution efficiency for chrysotile, amosite and crocidolite was calculated as 66.8%, 29.2% and 37.8%, respectively.

4. Discussion

4.1. Mineralogical Impact

Mineralogical and geochemical characterization of exposed asbestos-containing mine waste allows improved risk assessment with direct applications in predictive management. Mineral dust and fibres are heterogeneous substances with respiratory sensitizing properties. The complex nature and exposure to mineral fibres necessitate procedures that account for this complexity if the attenuation of the human health impacts is to be conducted reliably. Importantly, the selected methods are based on what is realistically practical for developing countries where funds and scientific engagement are limited. In hand sample, all three types of asbestos show asbestiform morphology, including fibre thickness, parallelism in arrangement, separability, and flexibility. The fibres retain their aspect ratio forming numerous finer fibres during breakage caused by crushing. All samples showed moderate cohesion as fibres were released from bulk material when vigorously disturbed by hand. The three types of asbestos minerals sampled are cross-fibres in veins for chrysotile and seams for the amphiboles.

The fibre geometry (Table 2), defined by its diameter (D) and length (L), is a key parameter in its pathogenicity, toxicity and inflammation [59,60]. Polarising light microscopy (PLM) is most used for semi-quantifying the percentage and identifying the type of fibre [61,62], but can also be used to accurately measure fibre dimensions $>1 \mu\text{m}$ in diameter [63,64]. The dimensions provide information on the respirability and biological activity of airborne fibres [65]. The ‘Stanton Hypothesis’ states that the optimum fibre morphology for generating intrapleural tumours is $D \leq 0.25 \mu\text{m}$ and $L > 8 \mu\text{m}$, and was derived from experimental observations succeeding fibre implantation and injection into animals [66]. According to this model, ‘frustrated phagocytosis’ [67] results because phagocytic cells are unable to eliminate ‘Stanton fibres’, i.e., needle-shaped particles with $L > 8 \mu\text{m}$ [66].

All samples consist of poly-filamentous fibre bundles with parallel-sided, long, thin fibres having straight extinction. Splayed ends and fibre curvature were characteristically demonstrated by the crocidolite samples. Under high magnification, amosite and crocidolite minerals do not appear compact having gaps and visible divisions between fibres further pointing to their asbestiform nature. Unlike amosite and crocidolite, individual chrysotile fibres are less clearly distinguishable under the polarising light microscope (PLM). Chrysotile appeared more compact; however, upon closer inspection, divisions between fibres were also identified, but less prominent than that of amosite and crocidolite. In PLM, the chrysotile fibres appear to be more tightly welded together with little porosity between them. Optically, the colours of the fibres are both homogenous and heterogenous under PLM.

Chemical heterogeneity suggested by colour variations in the fibre provides evidence of partial replacement of pre-existing fibres or generations of fibre growth. Homogenous colours were generally observed along the lengths of the amosite and crocidolite fibres (Figures S8, S10, S12 and S14). Heterogenous colours within individual fibres is only observed in chrysotile (Figures S4 and S6) and implies compositional variability. This is further documented under cross-polarising light (Figures S5 and S7). Both amphibole asbestos samples did not appear to show any modifications optically and texturally in PLM consistent with the homogenous colouring. In comparison with the amphibole asbestos samples, the chrysotile asbestos samples exhibit a more complex microstructure matrix under PLM, in which several coexisting textures are apparent.

The asbestos-containing rock materials are natural samples collected from mines, and thus, the presence of mineral impurities is expected [68,69]. Typically, natural asbestos-containing rock samples occurs with other non-asbestiform morphologies and minerals [70]. Although these associated phases are thought to be harmless, little information on their potential toxic effects exists [70]. Thus, the characterisation of natural assemblages should include all phases occurring with the suspected asbestos fibres [70]. The results obtained via XRD analysis facilitate the identification of co-occurring fine-grained minerals that are difficult to detect optically. Chrysotile (serpentine) and crocidolite (amphibole) samples are homogeneous containing no additional mineral phases. Amosite displays mineral phase heterogeneity and crystalline impurities of ~4.1% quartz (SiO_2) and ~1.4% sepiolite ($\text{Mg}_4\text{Si}_6\text{O}_{15} \cdot 6\text{H}_2\text{O}$). Fibrous and crystalline quartz (SiO_2) is known as a prolific cytotoxic particle that results in lung tumours upon inhalation [71]. The phyllosilicate mineral, sepiolite ($\text{Mg}_4\text{Si}_6\text{O}_{15} \cdot 6\text{H}_2\text{O}$), belongs to the mineral group hornblende and is characterised by a fibrous habit [72]. Given limited studies and inadequate evidence for the carcinogenic effects of sepiolite in humans, only few animal studies have suggested that sepiolite is to be included in the Group 3 carcinogen category [73].

A survey of the published literature indicates very limited research and knowledge exists regarding the carcinogenic and pathogenic effects of asbestos associated mineral phases following chronic inhalation. However, asbestos-associated mineral phases should not be neglected when considering the combined factors encompassing the toxicity of asbestos-containing mine-wastes.

4.2. Geochemical Impact

Of further importance is the ability to quantify the amount of potentially harmful elements that can potentially be released both into the environment and ingested by the human body. The high concentrations of Al, Mg, Mn and Fe are not unexpected as they are major rock forming elements and are among the primary constituents in sediments and soils [74]. One of the most important factors for fibre-induced patho-biological activity is the total iron content of the asbestos minerals [60,75]. Siderosis is caused by the inhalation of iron-bearing compounds [76]. As iron acts as a catalyst for reactions involving release of reactive oxygen species and lipid, protein and DNA damage, it is a significant property in determining asbestos toxicity [77]. Iron becomes available at the reacting surface of fibres

during dissolution where, through a Haber–Weiss chain reaction sequence, it promotes hydroxyl radical formation that damages DNA [78,79].

In addition to iron, other major chemical elements have been reported to participate in asbestos toxicity following inhalation [80,81]. Silicon (Si) is the second most abundant element, and when inhaled, this results in numerous pathologies such as silicosis [82]. Being the third most abundant element in the Earth's crust, the environmental toxicology of aluminium has been revealed in recent investigations to cause numerous diseases. It thus presents a major threat to plants, animals and humans [83,84]. The bulk chemical analysis of the chrysotile sample indicates only a slight deviation from the ideal composition of serpentine, containing very little Fe and Al. Substitution in chrysotile may occur in both the octahedral (O) and tetrahedral (T) sheets making up this layer silicate [85]. In the 1:1 T-and-O-sheet ratio, both Si^{4+} and Mg^{2+} can be replaced by Al^{3+} , respectively, with an average Al_2O_3 content of <0.9 wt.%, while the FeO content may be as much as 6 wt.% [86]. Mg^{2+} in the O sheet can also be replaced by Fe^{2+} and Fe^{3+} while Si^{4+} replacement in the T sheet is infrequent and minor. In the octahedral sheet, both Fe^{2+} and Fe^{3+} can replace Mg and the eventual replacement of Si^{4+} by Fe^{3+} may occur, although Al^{3+} is preferentially hosted in this position. The presence of both Fe^{2+} and Fe^{3+} exclusively in six-fold coordination has been suggested by [69].

The different samples show considerably variable Mn concentrations with the highest amount found in the amosite. These results concur with those reported in [87], which explained that Mg in all the M(1), M(2), M(3) and M(4) sites of magnesium-iron-manganese-lithium amphiboles may be substituted with Mn [11,12]. Manganese is an essential trace element for biological organisms. However, in excess, manganese poisoning ensues typically in the brain and lungs [88]. Thus, managing the environmental entrance and migration of manganese is a marked human health risk to humans [89].

Trace elements within mineral fibres may, in addition to the major elements, take part in the fibre toxicity [11,12,90–92]. The presence of trace metals in fibres and their effects on the carcinogenesis of asbestos has been documented by IARC, 2012 [93]. In our study, the highest content of Ni, Co, Cr and V was observed in chrysotile; amosite contained the greatest concentration of Zn, Rb, Sr, Zr, Nb and Ba; and crocidolite was the only sample in which Ga was measured. Overall, the amosite rock sample contained the greatest number of detected trace elements and crocidolite had the overall lowest concentration of trace elements. Mn and trace metals, such as Ni, Cr, Ni and Cu, in chrysotile almost exclusively represent isomorphous substitution of Mg [16,94,95]. Unlike that for antigorite and lizardite minerals, trace metal substitution in chrysotile is typically more restricted [96]. Interestingly, although characterised by different geological conditions of formation, the detection of Cu, Ni, Zn, Sr, Yt and Zr was shared by the three asbestos rock samples. Lead was detected in all samples, and is a considerably toxic metal [97]. Unlike other metals (e.g., copper, manganese, and zinc) lead serves no biological functions [97] and is highly toxic being listed as a hazardous heavy metal contaminant [98]. The toxicity of lead in living cells is caused by oxidative stress and ionic mechanisms [99,100]. Due to its high toxicity, lead is ranked among the 10 top priority substances of concern to the public (ATSDR, 2018). Several effects arise from the contamination of soil with lead including the reduction in soil fertility, microbial diversity and nutrients [98]. Nickel was detected in all samples with chrysotile exhibiting an exceptionally high concentration (1519 ppm). A variety of adverse human health effects, such as lung fibrosis, kidney diseases, contact dermatitis, cardiovascular diseases and cancer of the respiratory tract, are forms of nickel allergy that can result from contact with nickel compounds [101–103]. Bioavailable Ni^{2+} toxicity at the intracellular sites was postulated by [104]. In humans, CD4+T lymphocytes cause the greatest apoptosis and DNA damage, and caspase-9-positive T cells are induced by Ni^{2+} at a concentration of 0.05 mM [105].

Chromium was found in the chrysotile (83 ppm) and amosite (4.6 ppm) samples and represents a source of concern. Chromium results in the formation of hydroxyl and superoxide radicals described by the Fenton reaction [106]. Fenton reactions induced

by Cr^{3+} damage proteins [107]. The direct binding of Cr^{3+} to numerous non-metallo-proteins has been shown in Cr associated patients to result in the loss of their biological functions [108]. Chromium is also known to cause several health problems such as vomiting, kidney failure, mouth ulcers, lung cancer, stomach cancer, indigestion and acute tubular necrosis in humans following contact [109–111].

Vanadium was measured in chrysotile (16 ppm), crocidolite (3.9 ppm) and amosite (3.5 ppm) samples. Any of the three oxidation states of vanadium can produce genotoxic effects [112]. However, double-strand breaks are induced by V^{4+} causing lesions and creating aberrations in structural chromosomes [112,113]. Asthma, anaemia and rhinitis can be caused by excessive amounts of vanadium in the body and even increase the possibility of lung cancer and uraemia occurrence [114–117]. The release of vanadium from asbestos fibres into solution does not represent a concern as it is very low [112].

Molybdenum was measured in amosite (0.9 ppm). Biologically, molybdenum is an essential nutrient required by humans. However, inhalation and exposure to excess levels can decrease lung functioning, coughing and dyspnoea [118,119].

The substantial presence of potentially toxic trace elements at concentrations measured in the studied chrysotile and amphibole asbestos samples may be explained, primarily, because of isomorphic substitutions in particular crystallographic positions [94,120]. The variability in potentially toxic elements amongst the studied samples, on the other hand, is best explained by the shared chemical changeability exhibited by asbestos mineral particles [121] and the different petrological and geochemical processes occurring during their formation [122]. High levels of heavy metals in the wastes indicate the possibility of their release into the soil, water and atmospheric environments, presenting an interminable environmental hazard [123].

The heavy metals hosted in fibrous minerals accumulate in the lungs via dissolution following inhalation, altering the normal human lung baseline levels of these elements [124]. The surface area of asbestos has been proposed to play a role in fibre toxicity [125]. The surface area is a factor influencing the rate of dissolution and therefore clearance from the lungs [58,60]. Lung cancer, bronchogenic carcinoma, mesothelioma, etc., are caused when sufficient abundances of heavy metals are accumulated as the human lung tissue is damaged by metal-induced disease [11,12,76,92,124,126]. The concentration range of metals in normal human lungs are reported in Table 7; these ranges are greatly exceeded by their concentrations in the different asbestos types.

The solid mass loss of the bio-durability experiments for each asbestos sample is always less than 100% solid. The reason is not incomplete dissolution but rather the precipitation of silica out of the solution [23]. As demonstrated by the dissolution tests, chrysotile has the lowest bio-durability and amosite the highest. Based on the close link between bio-durability and bio-persistence, it is expected that amosite fibres will have a much longer retention time following inhalation when compared to both chrysotile and crocidolite. Therefore, amosite fibres have a greater toxicity than chrysotile and crocidolite following inhalation due to their greater persistence in the lungs [127].

More recently, in addition to the already stated mineralogical and geochemical properties influencing the toxicity to asbestos exposure, trace element concentrations hosted in asbestos mineral fibres and their role in fibre toxicity have come under the spotlight [122]. The obvious threat of exposure to asbestos is much publicised. Numerous rehabilitation strategies, focused solely on mitigating the dispersion of these mineral fibres, have been considered and implemented. As well as their role in determining fibre toxicity, the elevated concentrations of heavy metals hosted in asbestos minerals pose a profound influence on the quality of the environment. Many potentially toxic elements have been found to be hosted in all forms of asbestos minerals [128–130]. The fundamental factor surrounding these findings is that, in the natural setting, leaching, and weathering of asbestos-bearing rocks results in reduced heavy metal concentrations within the mineral particles themselves and the subsequent increase in concentrations in the surrounding soil and water ecosystems [130,131]. Compared to the maximum limits imposed by environmental governments

and agencies, the concentrations of heavy metals in the proximity of asbestos-bearing geological sites are typically one order of magnitude greater [132], as documented, for instance, in the serpentine-derived soils of the Gimigliano—Mount Reventino Unit (GMRU), Calabria Region (S-Italy) [133]. In addition to soils, the interaction of water with asbestos-bearing rocks is also characterised by exceedingly high heavy metal concentrations due to the dissolution of these minerals [19]. The magnitudes of their concentrations and the fact that these toxic elements can be mobilised and dispersed into different terrestrial environments and subsequently absorbed by humans, makes their presence in asbestos-bearing mine waste a consequential public health and environmental threat.

Table 7. Comparison of geochemical data in this study and the concentration range of heavy metal in normal human lungs (ppm).

Metals (ppm)	Chrysotile	Amosite	Crocidolite	Concentration Range of Trace Elements in Normal Human Lungs (ppm) [122]
Al	11,147.8	6802.1	1322.6	
Fe	13,988	289,340	267,940	40–500
Mn	230	4987	465	0.01–3
Mg	246,200	35,220	13,449	
Cr	83.4	4.61	D.L.	0.002–0.50
Co	52.55	D.L.	D.L.	0.002–0.1
Ni	1518.54	51.24	11.86	0.01–1.00
Cu	21.99	36.77	35	1–5.00
Zn	16.19	41.62	12.66	1–30.00
Zr	0.49	3.7	0.38	
Ba	D.L.	28.17	1.69	>1.10
Pb	6.62	5.32	5.06	0.02–0.50

4.3. Geographic Impact and Rehabilitation

Substantial volumes of crushed rock-based wastes were produced during the mining of asbestos mineral resources in Southern Africa. The geographic impact of these derelict asbestos mine sites is vast, littering the landscape across most of rural South and Southern Africa. The accumulation of these historical asbestos-mining rock wastes resulted in large unmanaged mine dumps characterised by poly-mineral and rock assemblages, which tend to be unstable and display unfavourable physical and hydrological properties under prevalent physico-chemical conditions that increase their potentially toxicity [134–136]. Despite the increasing recognition of environmental, health and safety risks associated with derelict asbestos mine sites many of them are exposed, unconfined and still to be rehabilitated. In the context of risk assessment and exposure scenarios in Southern Africa numerous difficulties are faced as statistical information regarding the health response and number of asbestos related disease suffers has not been properly documented and/or acknowledged. The lack of background data makes fully comprehending and assessing the extent of risks from these asbestos sites challenging. The ‘rehabilitation industry’ in South Africa commonly practices vegetation establishment primarily aimed to generate surface stability with the aim to re-establish and return the site to a functional and sustainable ecosystem [137]. The main, governmental, and environmental agencies involved in derelict asbestos-mine land management have adopted the soil remediation approach to evaluate the rehabilitation requirements [137]. Asbestos mine dumps demonstrate huge variation in physical, geochemical and mineralogical characteristics [138]. Given the site-specific nature of mine rock wastes a thorough investigation and characterisation is the first critical step for the formulation of a rehabilitation plan [139]. Individually and interactively, the

physical, mineralogical, and geochemical properties result in impediments and challenges to natural vegetation establishment during rehabilitation and its subsequent sustainability. The way asbestos mine dump rehabilitation is undertaken is based on the credence that ecological restoration and remediation on all derelict and post-mining terrains can be tackled and accomplished in short deadlines. This emphasises the lack of appreciation of the influence of geological conditions on the substrates, the community assembly and plant growth [140,141]. To predict the potential challenges to rehabilitation mineralogical and geochemical characterisation of asbestos mine waste should become a standard practice. Derelict asbestos mine sites in Southern Africa are a major issue due to the geographic expanse and their insufficient rehabilitation outcomes. To tackle this problem, greater attention and more research focus is required to understand how the edaphic conditions including geological factors hinder positive restorative outcomes and therefore impact progressive risk mitigation strategies. The potential exposure scenarios for communities surrounding derelict asbestos mine sites in Southern Africa are not as easily resolved for they include air, water and soil. As communities in these areas are rural and in large have livelihoods based on subsistence farming practices, their very existence is interconnected to the asbestos contaminated land in which they occupy. The complexities between the scientific and social aspects of derelict mine sites in Southern Africa make hazard and risk assessments more challenging compared to those of similar nature in developed countries. In such a context, specific scientific data and solutions to such environmental and human health issues require a paradigm shift for researchers developing solutions that have practical applicability to the location of interest.

5. Conclusions

Mineralogical and geochemical characterisations of asbestos mineral fibres left at derelict asbestos mine sites are important for two major reasons: firstly, to identify and assess their human health hazard and define the toxicity degree; secondly, to define the degree of potential environmental contamination in soils and (sub)surface waters in areas where these minerals occur. The results given in the study indicate that chrysotile, although being the least bio-durable, contains heavy metal concentrations that exceed those of the normal threshold concentrations in lungs beyond which result in functional respiratory problems. Amosite is of particular concern due to its high bio-durability and metal content above values of the safe lung-threshold. These high levels of heavy metals detected in both chrysotile and amosite are potentially harmful not only to human health, but also the environment in general, as they could contaminate the surrounding soil and water, which forms the basis of existence for rural communities in remote locations. To conclude, the cost-effective, reliable, and easily accessible analytical methods applied here substantiate that baseline values, pertinent to the geological material, require revision as very little data are currently reported in the literature and other official reports concerning South African regulations and guidelines.

Supplementary Materials: The following supporting information can be downloaded at: <https://www.mdpi.com/article/10.3390/min13101352/s1>, Figure S1: Sample Ch1 (A) Chrysotile rock sample; (B) length of fibres spanning the width of veins; (C) Individual masses of matted white fibres; and (D) parting at the centre of the vein width halving the length of the cross-vein fibres. Figure S2: Sample Am2 (A) amosite rock sample and (B) matted and splintery fibres. Figure S3: Sample Cr3 (A) crocidolite rock sample and (b) showing slight curvature of poly-filamentous bundles. Figure S4: Sample Ch1 chrysotile fibre bundle (PPL). Notice the break in the bundle in the top right. Figure S5: Sample Ch1 chrysotile fibre bundle (XPL). Figure S6: Sample Ch1. Partially altered chrysotile fibres shown by amorphous, irregular material and cloudiness (PPL). Figure S7: Sample Ch1. Partially altered chrysotile fibres shown by amorphous, irregular material and cloudiness (XPL). Figure S8: Sample Am2. Extremely fine amosite fibres showing parallel alignment and matting (PPL). Figure S9: Sample Am2. Extremely fine amosite fibres showing parallel alignment and matting (XPL). Figure S10: Sample Am2. Amosite fibres at maximum angle of pleochroism showing heterogenous colours (PPL). Figure S11: Sample Am2. Amosite fibres at maximum angle of birefringence showing heterogenous

interference colours (XPL). Figure S12: Sample Cr3. Poly-filamentous crocidolite (PPL). Figure S13: Sample Cr3. Poly-filamentous crocidolite (XPL). Figure S14: Sample Cr3. Crocidolite fibres with spayed ends (PPL). Figure S15: Sample Cr3. Crocidolite fibres with spayed ends (XPL). Graph S1: Diffractogram and relative phases (weight %) of the chrysotile sample. Graph S2: Diffractogram and relative phases (weight %) of the amosite sample. Graph S3: Diffractogram and relative phases (weight %) of the crocidolite sample. Table S1: The values of 2θ and intensity (I) recorded for each the peaks of each phase from the X-ray diffraction record (λ (CoK α) = 1.78892). Table S2: BET surface area report. Table S3: The dissolved mass fraction (DMF) calculated for the asbestos samples.

Author Contributions: J.S.S., S.M. and R.B. conceptualized the research; R.B. and S.M. provided PhD supervision to J.S.S.; J.S.S. collected samples; J.S.S. and A.H.W. carried out analyses; J.S.S. prepared original draft of manuscript; R.B., S.M. and A.H.W. reviewed and corrected various versions of the manuscript; R.B. and S.M. acquired funding. All authors have read and agreed to the published version of the manuscript.

Funding: Financial support was provided by the DSI-NRF Centre of Excellence for Integrated Mineral and Energy Resource Analysis (DSI-NRF CIMERA) as a PhD scholarship to J. S. Schapira.

Data Availability Statement: All data used are presented as supplemental files. Additional data is available from the lead author on request.

Acknowledgments: Opinions expressed, and conclusions arrived at, are those of the authors and are not to be attributed to the DSI-NRF CIMERA. Paul Nex is thanked for providing some of the sample material. Constructive comments from four anonymous reviewers are acknowledged.

Conflicts of Interest: The authors declare no conflict of interest.

References

1. Cornelissen, H.; Watson, I.; Adam, E.; Malefetse, T. Challenges and strategies of abandoned mine rehabilitation in South Africa: The case of asbestos mine rehabilitation. *J. Geochem. Explor.* **2019**, *205*, 106354. [[CrossRef](#)]
2. Harris, L.V.; Kahwa, I.A. Asbestos: Old foe in 21st century developing countries. *Sci. Total Environ.* **2003**, *307*, 1–9. [[CrossRef](#)]
3. Ndlovu, N.; teWater Naude, J.; Murray, J. Compensation for environmental asbestos-related diseases in South Africa: A neglected issue. *Glob. Health Action* **2013**, *6*, 82–88. [[CrossRef](#)] [[PubMed](#)]
4. Williams, C.; Dell, L.; Adams, R.; Rose, T.; Van Orden, D.R. State-of-the-science assessment of non-asbestos amphibole exposure: Is there a cancer risk? *Environ. Geochem. Health* **2013**, *35*, 357–377. [[CrossRef](#)] [[PubMed](#)]
5. Hodgson, A.A. Nature and paragenesis of asbestos minerals. *Philos. Trans. R. Soc. Lond. A* **1977**, *286*, 611–624.
6. Okayasu, R.; Takahashi, S.; Yamada, S.; Hei, T.K.; Ullrich, R.L. Asbestos and DNA double strand breaks. *Cancer Res.* **1999**, *59*, 298–300. [[PubMed](#)]
7. Kilburn, K.H. Indoor air effects after building renovation and in manufactured homes. *Am. J. Med. Sci.* **2000**, *320*, 249–254. [[CrossRef](#)]
8. Unfried, K.; Schurkes, C.; Abel, J. Distinct spectrum of mutations induced by crocidolite asbestos clue for 8-hydroxydeoxyguanosine-dependent mutagenesis in vivo. *Cancer Res.* **2002**, *62*, 99–104.
9. Mossman, B.T.; Lippmann, M.; Hesterberg, T.W.; Kelsey, K.T.; Barchowsky, A.; Bonner, J.C. Pulmonary endpoints (lung carcinomas and asbestosis) following inhalation exposure to asbestos. *J. Toxicol. Environ. Health* **2011**, *14*, 76–121. [[CrossRef](#)]
10. Pugnali, A.; Giantomassi, F.; Lucarini, G.; Capella, S.; Bloise, A.; Di Primio, R.; Belluso, E. Cytotoxicity induced by exposure to natural and synthetic tremolite asbestos: An in vitro pilot study. *Acta Histochem.* **2013**, *115*, 100–112. [[CrossRef](#)]
11. Bloise, A.; Barca, D.; Gualtieri, A.F.; Pollastri, S.; Belluso, E. Trace elements in hazardous mineral fibres. *Environ. Pollut.* **2016**, *216*, 314–323. [[CrossRef](#)] [[PubMed](#)]
12. Bloise, A.; Punturo, R.; Catalano, M.; Miriello, D.; Cirrincione, R. Naturally occurring asbestos (NOA) in rock and soil and relation with human activities: The monitoring example of selected sites in Calabria (southern Italy). *Ital. J. Geosci.* **2016**, *135*, 268–279. [[CrossRef](#)]
13. Bloise, A.; Catalano, M.; Gualtieri, A.F. Effect of grinding on chrysotile, amosite and crocidolite and implications for thermal treatment. *Minerals* **2018**, *8*, 135. [[CrossRef](#)]
14. Harper, M. 10th Anniversary critical review: Naturally occurring asbestos. *J. Environ. Monit.* **2008**, *10*, 1394–1408. [[CrossRef](#)]
15. Culley, M.R.; Zorland, J.; Freire, K. Community responses to naturally occurring asbestos: Implications for public health practice. *Health Educ. Res.* **2010**, *25*, 877–891. [[CrossRef](#)]
16. Bloise, A.; Belluso, E.; Critelli, T.; Catalano, M.; Apollaro, C.; Miriello, D.; Barrese, E. Amphibole asbestos and other fibrous minerals in the meta-basalt of the gimigliano-mount reventino unit (Calabria, South-Italy). *Rend. Online Soc. Geol. Ital.* **2012**, *21*, 847–848.

17. Bloise, A.; Critelli, T.; Catalano, M.; Apollaro, C.; Miriello, D.; Croce, A.; Barrese, E.; Liberi, F.; Piluso, E.; Rinaudo, C.; et al. Asbestos and other fibrous minerals contained in the serpentinites of the Gimigliano-Mount Reventino Unit (Calabria, S-Italy). *Environ. Earth Sci.* **2014**, *71*, 3773–3786. [\[CrossRef\]](#)
18. Punturo, R.; Ricchiuti, C.; Mengel, K.; Apollaro, C.; De Rosa, R.; Bloise, A. Serpentine-derived soils in southern Italy: Potential for hazardous exposure. *J. Mediterr. Earth Sci.* **2018**, *10*, 51–61.
19. Apollaro, C.; Fuoco, I.; Vespasiano, G.; De Rosa, R.; Cofone, F.; Miriello, D.; Bloise, A. Geochemical and mineralogical characterization of tremolite asbestos contained in the Gimigliano-Monte Reventino Unit (Calabria, south Italy). *J. Mediterr. Earth Sci.* **2018**, *10*, 5–15.
20. Braun, L.; Kisting, S. Asbestos-Related Disease in South Africa: The Social Production of an Invisible Epidemic. *Am. J. Public Health* **2006**, *96*, 1386–1396. [\[CrossRef\]](#) [\[PubMed\]](#)
21. Rees, D.; Myers, J.E.; Goodman, K.; Fourie, E.; Blignaut, C.; Chapman, R.; Bachmann, M.O. Case-Control Study of Mesothelioma in South Africa. *Am. J. Ind. Med.* **1999**, *35*, 213–222. [\[CrossRef\]](#)
22. Ramazzini, C. The global health dimensions of asbestos and asbestos related diseases. *J. Occup. Health* **2011**, *58*, 220–223. [\[CrossRef\]](#)
23. Gualtieri, A.F.; Viani, A.; Sgarbi, G.; Lusvardi, G. In vitro biodurability of the product of thermal transformation of cement-asbestos. *J. Hazard. Mater.* **2012**, *205–206*, 63–71. [\[CrossRef\]](#) [\[PubMed\]](#)
24. Fubini, B.; Otero-Arèan, C. Chemical aspects of the toxicity of inhaled mineral dusts. *Chem. Soc. Rev.* **1999**, *28*, 373–381. [\[CrossRef\]](#)
25. Fubini, B.; Bolis, V.; Cavenago, A.; Volante, M. Physicochemical properties of crystalline silica dusts and their possible implication in various biological responses. *Scand. J. Work Environ. Health* **1995**, *21*, 9–15. [\[PubMed\]](#)
26. Higuera, P.; Oyarzun, R.; Iraizoz, J.M.; Lorenzo, S.; Esbrí, J.M.; Martínez-Coronado, A. Low-cost geochemical surveys for environmental studies in developing countries: Testing a field portable XRF instrument under quasi-realistic conditions. *J. Geochem. Explor.* **2012**, *113*, 3–12. [\[CrossRef\]](#)
27. Anhaeusser, C.R. The nature of chrysotile asbestos occurrences in southern Africa: A review. *Econ. Geol.* **1976**, *71*, 96–116. [\[CrossRef\]](#)
28. Hunter, D.R.; Jones, D.H. *Geological Map Series (1:25,000)*; Sheet 2; Swaziland Geological Survey: Piggs Peak, Swaziland, 1969.
29. Viljoen, R.P.; Viljoen, M.J. The geology and geochemistry of the layered ultramafic bodies of the Kaapmuiden area, Barberton Mountain Land. *Geol. Soc. S. Afr. Spec. Publ.* **1969**, *1*, 661–688.
30. Biljon, V. The chrysotile deposits of the eastern Transvaal and Swaziland. In *The Geology of Some Ore Deposits in Southern Africa*; Haughton, S.H., Ed.; Geological Society of South Africa: Johannesburg, South Africa, 1964; pp. 625–669.
31. Abbott, P. A Review of Asbestos Resources. Master Thesis, Rhodes University, Grahamstown, South Africa, 1983.
32. Hart, H.P. Asbestos in South Africa. *J.S. Afr. Inst. Min. Metall.* **1988**, *88*, 185–198.
33. Riordon, P.H. The genesis of asbestos in ultrabasic rocks. *Econ. Geol.* **1955**, *50*, 67–81. [\[CrossRef\]](#)
34. Cairncross, B. *Field Guide to Rocks and Minerals of Southern Africa*; Struik Nature: Cape Town, South Africa, 2004.
35. Dreyer, C.J.B.; Sohnge, A.P.G. *The Crocidolite and Amosite Deposits of the Republic of South Africa and Bophuthatswana*; Handbook; Geological Survey of South Africa: Pretoria, South Africa, 1992; Volume 12, p. 126.
36. Miyano, T.; Beukes, N.J. Mineralogy and Petrology of the Contact Metamorphosed Amphibole Asbestos-bearing Penge Iron Formation, Eastern Transvaal, South Africa. *J. Petrol.* **1997**, *38*, 651–676. [\[CrossRef\]](#)
37. Genis, J.H. The Genesis of the Blue Amphibole Asbestos of the Union of South Africa. Ph.D. Thesis, University of Cape Town, Cape Town, South Africa, 1961.
38. Reinecke, L.; McClure, L. Variations in the quality of amosite asbestos at Penge, Transvaal. *Trans. Geol. Soc. S. Afr.* **1933**, *36*, 29–39.
39. Howling, G.E. *Asbestos*; Imperial Institute: London, UK, 1937; p. 88.
40. Strohmeier, B.R.; Huntington, J.C.; Bunker, K.L.; Sanchez, M.S.; Allison, K.; Lee, R.J. What is asbestos and why is it important? Challenges of defining and characterizing asbestos. *Int. Geol. Rev.* **2010**, *52*, 801–872. [\[CrossRef\]](#)
41. Plumlee, G.S.; Morman, S.A.; Ziegler, T.L. The toxicological geochemistry of earth minerals: An overview of processes and the interdisciplinary methods used to understand them. *Rev. Mineral. Geochem.* **2006**, *64*, 5–57. [\[CrossRef\]](#)
42. Ilgren, E.B. The fiber length of coalinga chrysotile: Enhanced clearance due to its short nature in aqueous solution with a brief critique on ‘Short Fiber Toxicity’. *Indoor Built Environ.* **2008**, *17*, 5–26. [\[CrossRef\]](#)
43. Rietveld, H.M. The Rietveld method. *Physica Scripta* **2014**, *89*, 098002. [\[CrossRef\]](#)
44. Norrish, K.; Hutton, J.T. An accurate X-ray spectrographic method for the analysis of geologic samples. *Geochem. Et Cosmochim. Acta* **1969**, *33*, 431–454. [\[CrossRef\]](#)
45. Wilson, A.H. A chill sequence to the Bushveld Complex: Insight into the first stage of emplacement and implications for the parental magmas. *J. Petrol.* **2012**, *53*, 1123–1168. [\[CrossRef\]](#)
46. Bismarck, A.; Aranberri-Askargorta, I.; Springer, J.; Lampke, T.; Wielage, B.; Stamboulis, A.; Shenderovich, I.; Limbach, H.-H. Surface Characterization of Flax, Hemp and Cellulose Fibers; Surface Properties and the Water Uptake Behavior. *Polym. Compos.* **2002**, *23*, 872–894. [\[CrossRef\]](#)
47. Boulanger, G.; Andujar, P.; Pairen, J.-C.; Billon-Galland, M.-A.; Dion, C.; Dumortier, P.; Brochard, P.; Sobaszek, A.; Bartsch, P.; Paris, C.; et al. Quantification of short and long asbestos fibers to assess asbestos exposure: A review of fiber size toxicity. *Environ. Health* **2014**, *13*, 59. [\[CrossRef\]](#) [\[PubMed\]](#)

48. Gualtieri, A.F. Bridging the gap between toxicity and carcinogenicity of mineral fibres by connecting the fibre crystal-chemical and physical parameters to the key characteristics of cancer. *Curr. Res. Toxicol.* **2021**, *2*, 42–52. [\[CrossRef\]](#)
49. Brunauer, S.; Emmett, P.H.; Teller, E. Adsorption of gases in multimolecular layers. *J. Am. Chem. Soc.* **1938**, *60*, 309–319. [\[CrossRef\]](#)
50. Aust, A.E.; Cook, P.M.; Dodson, R.F. Morphological and chemical mechanisms of elongated mineral particle toxicities. *J. Toxicol. Environ. Health Part B* **2011**, *14*, 40–75. [\[CrossRef\]](#)
51. Deng, Z.J.; Liang, M.L.; Tóth, I.; Monteiro, M.J.; Michin, R.F. Molecular interaction of poly (acrylic acid) gold nanoparticles with human fibrinogen. *ACS Nano* **2012**, *6*, 8962–8969. [\[CrossRef\]](#)
52. Di Giuseppe, D. Characterization of Fibrous Mordenite: A First Step for the Evaluation of Its Potential Toxicity. *Crystals* **2020**, *10*, 769. [\[CrossRef\]](#)
53. Kaszuba, J.; Yardley, B.; Andreani, M. Experimental perspectives of mineral dissolution and precipitation due to carbon dioxide-water-rock interactions. *Rev. Mineral. Geochem.* **2013**, *77*, 153–188. [\[CrossRef\]](#)
54. Oze, C.; Solt, K.-L. Biodurability of chrysotile and tremolite asbestos in simulated lung and gastric fluids. *Am. Mineral.* **2010**, *95*, 825–831. [\[CrossRef\]](#)
55. Rozalen, M.; Huertas, F.J. Comparative effect of chrysotile leaching in nitric, sulfuric and oxalic acid at room temperature. *Chem. Geol.* **2013**, *352*, 134–142. [\[CrossRef\]](#)
56. Rozalen, M.; Ramos, M.E.; Gervilla, F.; Kerestedjian, T.; Fiore, S.; Huertas, F.J. Dissolution study of tremolite and anthophyllite: pH effect on the reaction kinetics. *Appl. Geochem.* **2014**, *49*, 46–56. [\[CrossRef\]](#)
57. Karunaratne, P.C.T.; Fernando, G.W.A.R. Characterisation and radiation impact of corrugated asbestos roofing sheets in Sri Lanka. *J. Geol. Soc. Sri Lanka* **2015**, *17*, 31–40.
58. Fischer, C.; Kurganskaya, I.; Schäfer, T.; Lüttge, A. Variability of crystal surface reactivity: What do we know? *Appl. Geochem.* **2014**, *43*, 132–157. [\[CrossRef\]](#)
59. Donaldson, K.; Murphy, F.A.; Duffin, R.; Poland, C.A. Asbestos, carbon nanotubes and the pleural mesothelium: A review of the hypothesis regarding the role of long fibre retention in the parietal pleura, inflammation and mesothelioma. *Fibre Tox.* **2010**, *7*, 5. [\[CrossRef\]](#) [\[PubMed\]](#)
60. Gualtieri, A.F. Towards a quantitative model to predict the toxicity/pathogenicity potential of mineral fibers. *Toxicol. Appl. Pharmacol.* **2018**, *361*, 89–98. [\[CrossRef\]](#)
61. McCrone, W.; McCrone, L.; Delly, J. *Polarized Light Microscopy*; Ann Arbor Science Publishers, Inc.: Ann Arbor, MI, USA, 1978.
62. Middleton, A.P. The identification of asbestos in solid materials. In *Asbestos: Properties Applications and Hazards*; Michaels, L., Chissick, S.S., Eds.; John Wiley and Sons, Inc.: Chichester, UK, 1979.
63. Vaughan, N.P.; Rooker, S.J.; LeGuen, J.M. In situ identification of asbestos fibres collected on membrane filters for counting. *Ann. Occup. Hyg.* **1981**, *24*, 281–290.
64. Bernstein, D.; Dunnigan, J.; Hesterberg, T.; Brown, R.; Velasco, J.A.L.; Barrera, R.; Hoskins, J.; Gibbs, A. Health risk of chrysotile revisited. *Crit. Rev. Toxicol.* **2013**, *43*, 154–183. [\[CrossRef\]](#)
65. Walton, W.H. The nature, hazards, and assessment of occupational exposure to airborne asbestos dust: A review. *Ann. Occup. Hyg.* **1982**, *25*, 117–247.
66. Stanton, M.F.; Layard, M.; Tegeris, A.; Miller, E.; May, M.; Morgan, E.; Smith, A. Relation of particle dimension to carcinogenicity in amphibole asbestoses and other fibrous minerals. *J. Natl. Cancer Inst.* **1981**, *67*, 965–975. [\[PubMed\]](#)
67. Churg, A. Asbestos lung burden and disease patterns in man. In *Health Effects of Mineral Dust. Review in Mineralogy and Geochemistry*; Guthrie, G.D., Mossman, B.T., Eds.; Mineralogical Society of America: Chantilly, VA, USA, 1993; Volume 28, pp. 409–426.
68. Pollastri, S.; Gualtieri, A.F.; Gualtieri, M.L.; Hanuskova, M.; Cavallo, A.; Gaudino, G. The zeta potential of mineral fibers. *J. Hazard. Mater.* **2014**, *276*, 469–479. [\[CrossRef\]](#) [\[PubMed\]](#)
69. Pollastri, S.; D’Acapito, F.; Trapananti, A.; Colantoni, I.; Andreozzi, G.B.; Gualtieri, A.F. The chemical environment of iron in mineral fibers. A combined X-ray absorption and Mossbauer spectroscopic study. *J. Hazard. Mater.* **2015**, *298*, 282–293. [\[CrossRef\]](#) [\[PubMed\]](#)
70. Vigliaturo, R.; Ventura, G.D.; Choi, J.K.; Marengo, A.; Lucci, F.; O’Shea, M.J.; Pérez-Rodríguez, I.; Gieré, R. Mineralogical Characterization and Dissolution Experiments in Gamble’s Solution of Tremolitic Amphibole from Passo di Caldenno (Sondrio, Italy). *Minerals* **2018**, *8*, 557. [\[CrossRef\]](#) [\[PubMed\]](#)
71. Oberdörster, G. Toxicokinetics and effects of fibrous and nonfibrous particles. *Inhal. Toxicol.* **2002**, *14*, 29–56. [\[CrossRef\]](#)
72. Singer, A.; Kirsten, W.F.A.; Buhmann, C. Occurrence of sepiolite in the northern Transvaal, South Africa. *S. Afr. J. Geol.* **1992**, *95*, 165–170.
73. Turci, T.; Tomatis, M.; Pacella, A. Surface and bulk properties of mineral fibres relevant to toxicity. *Eur. Mineral. Union Notes Mineral.* **2017**, *18*, 171–214.
74. Iqbal, J.; Shah, M.H. Occurrence, risk assessment, and source apportionment of heavy metals in surface sediments from Khanpur Lake, Pakistan. *J. Anal. Sci. Technol.* **2014**, *5*, 28–32. [\[CrossRef\]](#)
75. Gualtieri, A.F.; Pollastri, S.; Gandolfi, N.B.; Gualtieri, M.L. In vitro acellular dissolution of mineral fibres: A comparative study. *Sci. Rep.* **2018**, *8*, 7071. [\[CrossRef\]](#) [\[PubMed\]](#)
76. Nemery, B. Metal toxicity and the respiratory tract. *Eur. Respir. J.* **1990**, *3*, 202–219. [\[CrossRef\]](#)
77. Fubini, B.; Mollo, L. Role of iron in the reactivity of mineral fibers. *Toxicol. Lett.* **1995**, *82/83*, 951–960. [\[CrossRef\]](#)

78. Gazzano, E.; Foresti, E.; Lesci, I.G.; Tomatis, M.; Riganti, C.; Fubini, B.; Roveri, N.; Ghigo, D. Different cellular responses evoked by natural and stoichiometric synthetic chrysotile asbestos. *Toxicol. Appl. Pharmacol.* **2005**, *206*, 356–364. [\[CrossRef\]](#) [\[PubMed\]](#)
79. Gazzano, E.; Turci, F.; Foresti, E.; Putzu, M.G.; Aldieri, E.; Silvagno, F.; Lesci, I.G.; Tomatis, M.; Riganti, C.; Romano, C.; et al. Iron loaded synthetic chrysotile: A new model solid for studying the role of iron in asbestos toxicity. *Chem. Res. Toxicol.* **2007**, *20*, 380–387. [\[CrossRef\]](#) [\[PubMed\]](#)
80. Shimizu, Y.; Dobashi, K.; Kusakbe, T.; Nagamine, T.; Oikawa, M.; Satoh, T.; Haga, J.; Ishii, Y.; Ohkubo, T.; Kamiya, T.; et al. In-air micro-particle induced X-ray emission analysis of asbestos and metals in lung tissue. *Int. J. Immunopathol. Pharmacol.* **2008**, *21*, 567–576. [\[CrossRef\]](#)
81. Nakamura, E.; Makishima, A.; Hagino, K.; Okabe, K. Accumulation of radium in ferruginous protein bodies formed in lung tissue: Association of resulting radiation hotspots with malignant mesothelioma and other malignancies. *Proc. Jpn. Acad. Ser. B Phys. Biol. Sci.* **2009**, *85*, 229–239. [\[CrossRef\]](#)
82. Hamilton, R.F., Jr.; Thakur, S.A.; Holian, A. Silica binding and toxicity in alveolar macrophages. *Free Radic. Biol. Med.* **2008**, *44*, 1246–1258. [\[CrossRef\]](#) [\[PubMed\]](#)
83. Barabasz, W.; Albinska, D.; Jaskowska, M.; Lipiec, J. Ecotoxicology of Aluminium. *Pol. J. Environ. Stud.* **2002**, *11*, 199–203.
84. Gupta, N.; Gaurav, S.S.; Kumar, A. Molecular Basis of Aluminium Toxicity in Plants: A Review. *Am. J. Plant Sci.* **2013**, *4*, 21–37. [\[CrossRef\]](#)
85. Deer, W.A.; Howie, R.A.; Zussman, J. Rock Forming Minerals. 3B. In *Layered Silicates Excluding Micas and Clay Minerals*, 2nd ed.; The Geological Society: London, UK, 2009.
86. Wicks, F.J.; Plant, A.G. Electron-Microprobe and X-Ray-Microbeam studies of serpentine textures. *Can. Mineral.* **1979**, *17*, 785–830.
87. Oberti, R.; Hawthorne, F.C.; Cannillo, E.; Camara, F. Longrange order in amphiboles. In *Amphiboles: Crystal Chemistry, Occurrence, and Health Issues*; Hawthorne, F.C., Oberti, R., Della Ventura, G., Mottana, A., Eds.; Mineralogical Society of America: Chantilly, VA, USA, 2007; pp. 125–172.
88. Hudnell, H.K. Effects from environmental Mn exposures: A review of the evidence from non-occupational exposure studies. *Neurotoxicology* **1999**, *20*, 379–398. [\[PubMed\]](#)
89. Aschner, J.L.; Aschner, M. Nutritional aspects of manganese homeostasis. *Mol. Asp. Med.* **2005**, *26*, 353–362. [\[CrossRef\]](#)
90. Fukuda, H.; Ebara, M.; Yamada, H.; Arimoto, M.; Okabe, S.; Obu, M.; Yoshikawa, M.; Sugiura, N.; Saisho, H. Trace elements and cancer. *Jpn. Med. Assoc. J.* **2004**, *47*, 391–395.
91. Bargagli, E.; Monaci, F.; Bianchi, N.; Bucci, C.; Rottoli, P. Analysis of trace elements in bronchoalveolar lavage of patients with diffuse lung diseases. *Biol. Trace Elem. Res.* **2008**, *124*, 225–235. [\[CrossRef\]](#)
92. Wei, B.; Yang, L.; Zhu, O.; Yu, J.; Jia, X. Multivariate analysis of trace elements distribution in hair of pleural plaques patients and health group in a rural area from China. *Hair Ther. Transplant. J.* **2014**, *4*, 2167–3118. [\[CrossRef\]](#)
93. IARC. *A Review of Human Carcinogens. Part C: Arsenic, Metals, Fibers, and Dusts*; International Agency for Research on Cancer: Lyon, France, 2012.
94. Bloise, A.; Barrese, E.; Apollaro, C. Hydrothermal alteration of Ti-doped forsterite to chrysotile and characterization of the resulting chrysotile fibers. *Neues Jahrb. Fur Mineral. Abh.* **2009**, *185*, 297–304. [\[CrossRef\]](#)
95. Bloise, A.; Belluso, E.; Fornero, E.; Rinaudo, C.; Barrese, E.; Capella, S. Influence of synthesis conditions on growth of Ni-doped chrysotile. *Microporous Mesoporous Mater.* **2010**, *132*, 239–245. [\[CrossRef\]](#)
96. Wicks, F.J.; O'Hanley, D.S. Serpentine minerals; structures and petrology. *Rev. Mineral. Geochem.* **1988**, *19*, 91–167.
97. Jaishankar, M.; Tseten, T.; Anbalagan, N.; Mathew, B.B.; Beeregowda, K.N. Toxicity, mechanism and health effects of some heavy metals. *Interdiscip. Toxicol.* **2014**, *7*, 60–72. [\[CrossRef\]](#)
98. Alengebawry, A.; Abdelkhalek, S.T.; Qureshi, S.R.; Wang, M.Q. Heavy Metals and Pesticides Toxicity in Agricultural Soil and Plants: Ecological Risks and Human Health Implications. *Toxics* **2021**, *9*, 42. [\[CrossRef\]](#)
99. Mathew, B.B.; Tiwari, A.; Jatawa, S.K. Free radicals and antioxidants: A review. *J. Pharm. Res.* **2011**, *4*, 4340–4343.
100. Wadhwa, N.; Mathew, B.B.; Jatawa, S.; Tiwari, A. Lipid peroxidation: Mechanism, models and significance. *Int. J. Curr. Sci.* **2012**, *3*, 29–38.
101. Oller, A.R.; Costa, M.; Oberdörster, G. Carcinogenicity assessment of selected nickel compounds. *Toxicol. Appl. Pharmacol.* **1997**, *143*, 152–166. [\[CrossRef\]](#) [\[PubMed\]](#)
102. McGregor, D.B.; Baan, R.A.; Partensky, C.; Rice, J.M.; Wilbourn, J.D. Evaluation of the carcinogenic risks to humans associated with surgical implants and other foreign bodies—A report of an IARC Monographs Programme Meeting. *Eur. J. Cancer* **2000**, *36*, 307–313. [\[CrossRef\]](#)
103. Seilkop, S.K.; Oller, A.R. Respiratory cancer risks associated with low-level nickel exposure: An integrated assessment based on animal, epidemiological, and mechanistic data. *Regul. Toxicol. Pharmacol.* **2003**, *37*, 173–190. [\[CrossRef\]](#)
104. Horie, M.; Nishio, K.; Fujita, K.; Kato, H.; Nakamura, A.; Kinugasa, S.; Endoh, S.; Miyauchi, A.; Yamamoto, K.; Murayama, H.; et al. Ultrafine NiO particles induce cytotoxicity in vitro by cellular uptake and subsequent Ni(II) release. *Chem. Res. Toxicol.* **2009**, *22*, 1415–1426. [\[CrossRef\]](#) [\[PubMed\]](#)
105. Caicedo, M.; Jacobs, J.J.; Reddy, A.; Hallab, N.J. Analysis of metal ion-induced DNA damage, apoptosis, and necrosis in human (Jurkat) T-cells demonstrates Ni²⁺ and V³⁺ are more toxic than other metals: Al³⁺, Be²⁺, Co²⁺, Cr³⁺, Cu²⁺, Fe³⁺, Mo⁵⁺, Nb⁵⁺, Zr²⁺. *J. Biomed. Mater. Res.* **2007**, *84*, 905–913. [\[CrossRef\]](#) [\[PubMed\]](#)

106. Briffa, J.; Sinagra, E.; Blundell, R. Heavy metal pollution in the environment and their toxicological effects on humans. *Heliyon* **2020**, *6*, e04691. [\[CrossRef\]](#)
107. Scharf, B.; Clement, C.C.; Zolla, V.; Perino, G.; Yan, B.; Elci, G.; Purdue, E.; Goldring, S.; Macaluso, F.; Cobelli, N.; et al. Molecular analysis of chromium and cobalt-related toxicity. *Sci. Rep.* **2014**, *4*, 5729. [\[CrossRef\]](#)
108. Gualtieri, A.F.; Andreozzi, G.B.; Tomatis, M.; Turci, F. Iron from a geochemical viewpoint. Understanding toxicity/pathogenicity mechanisms in iron-bearing minerals with a special attention to mineral fibers. *Free Radic. Biol. Med.* **2019**, *133*, 21–37. [\[CrossRef\]](#)
109. O'Flaherty, E.J. A physiologically-based model of chromium kinetics in the rat. *Toxicol. Appl. Pharmacol.* **1996**, *138*, 54–64. [\[CrossRef\]](#)
110. Beaumont, J.J.; Sedman, R.M.; Reynolds, S.D.; Sherman, C.D.; Li, L.H.; Howd, R.A.; Sandy, M.S.; Zeise, L.; Alexeeff, G.V. Cancer mortality in a Chinese population exposed to hexavalent chromium in drinking water. *Epidemiology* **2008**, *19*, 12–23. [\[CrossRef\]](#) [\[PubMed\]](#)
111. Shekhawat, K.; Chatterjee, S.; Joshi, B. Chromium Toxicity and its Health Hazards. *Int. J. Adv. Res.* **2015**, *3*, 167–172.
112. Gualtieri, A.F.; Lusvardi, G.; Zoboli, A.; Di Giuseppe, D.; Gualtieri, M.L. Biodurability and release of metals during the dissolution of chrysotile, crocidolite and fibrous erionite. *Environ. Res.* **2019**, *171*, 550–557. [\[CrossRef\]](#)
113. Rodríguez-Mercado, J.J.; Mateos-Nava, R.A.; Altamirano-Lozano, M.A. DNA damage induction in human cells exposed to vanadium oxides in vitro. *Toxicol. In Vitro* **2011**, *25*, 1996–2002. [\[CrossRef\]](#) [\[PubMed\]](#)
114. WHO. *Environmental Health Criteria 81: Vanadium*; WHO: Geneva, Switzerland, 1990; pp. 1–35.
115. WHO. *Vanadium Pentoxide and other Inorganic Vanadium Compounds*; Concise International Chemical Assessment Document: 29; WHO: Geneva, Switzerland, 2001.
116. ATSDR (Agency for Toxic substances and Disease Registry). *Draft Toxicological Profile for Several Trace Elements*; US Dept. Health Human Services, Agency for Toxic Substances and Disease Registry: Atlanta, GA, USA, 2002.
117. Crans, D.C.; Smee, J.J.; Gaidamauskas, E.; Yang, L. The chemistry and biochemistry of vanadium and the biological activities exerted by vanadium compounds. *Chem. Rev.* **2004**, *104*, 849–902. [\[CrossRef\]](#) [\[PubMed\]](#)
118. Chan, P.C.; Herbert, R.A.; Roycroft, J.H.; Haseman, J.K.; Grumbein, S.L.; Miller, R.A.; Chouf, B.J. Lung Tumor Induction by Inhalation Exposure to Molybdenum Trioxide in Rats and Mice. *Toxicol. Sci.* **1998**, *45*, 58–65. [\[CrossRef\]](#) [\[PubMed\]](#)
119. Ott, H.C.; Prior, C.; Herold, M.; Riha, M.; Laufer, G.; Ott, G. Respiratory symptoms and bronchoalveolar lavage abnormalities in molybdenum exposed workers. *Wien. Klin. Wochenschr.* **2004**, *116*, 25–30. [\[PubMed\]](#)
120. Ballirano, P.; Bloise, A.; Gualtieri, A.F.; Lezzerini, M.; Pacella, A.; Perchiazzi, N.; Dogan, M.; Dogan, A.U. The crystal structure of mineral fibres. In *Mineral Fibres: Crystal Chemistry, Chemical Physical Properties, Biological Interaction and Toxicity*; Gualtieri, A.F., Ed.; European Mineralogical Union and the Mineralogical Society of Great Britain & Ireland: London, UK, 2017; Volume 18, pp. 17–64.
121. Andreozzi, G.B.; Ballirano, P.; Gianfagna, A.; Mazziotti-Tagliani, S.; Pacella, A. Structural and spectroscopic characterization of a suite of fibrous amphiboles with high environmental and health relevance from Biancavilla (Sicily, Italy). *Am. Mineral.* **2009**, *94*, 1333–1340. [\[CrossRef\]](#)
122. Bloise, A.; Ricchiuti, C.; Punturo, R.; Pereira, D. Potentially toxic elements (PTEs) associated with asbestos chrysotile, tremolite and actinolite in the Calabria region (Italy). *Chem. Geol.* **2020**, *558*, 119896. [\[CrossRef\]](#)
123. Lu, S.; Wang, Y.; Teng, Y.; Yu, X. Heavy metal pollution and ecological risk assessment of the paddy soils near a zinc-lead mining area in Hunan. *Env. Monit Assess* **2015**, *187*, 627. [\[CrossRef\]](#)
124. Vanoeteren, C.; Cornelis, R.; Verbeeck, P. Evaluation of trace elements in human lung tissue III. *Corresp. Analysis. Sci. Total Environ.* **1986**, *54*, 237–245. [\[CrossRef\]](#) [\[PubMed\]](#)
125. Lippmann, M. Asbestos Exposure Indices. *Environ. Res.* **1988**, *48*, 86–106. [\[CrossRef\]](#) [\[PubMed\]](#)
126. Dixon, J.R.; Lowe, D.B.; Richards, D.E.; Cralley, L.J.; Stokinger, H.E. The role of trace metals in chemical carcinogenesis: Asbestos cancers. *Cancer Res.* **1970**, *30*, 1068–1074. [\[PubMed\]](#)
127. Visonà, S.D.; Capella, S.; Bodini, S.; Borrelli, P.; Villani, S.; Crespi, E.; Colosio, C.; Previderè, C.; Belluso, E. Evaluation of Deposition and Clearance of Asbestos (Detected by SEM-EDS) in Lungs of Deceased Subjects Environmentally and/or Occupationally Exposed in Broni (Pavia, Northern Italy). *Front. Public Health* **2021**, *9*, 678040. [\[CrossRef\]](#)
128. Scambelluri, M.; Piccardo, G.B.; Philippot, P.; Robbiano, A.; Negretti, L. High salinity fluid inclusions formed from recycled seawater in deeply subducted alpine serpentinite. *Earth Planet. Sci. Lett.* **1997**, *148*, 485–499. [\[CrossRef\]](#)
129. Tiepolo, M.; Oberti, R.; Zanetti, A.; Vannucci, R.; Foley, S.F. Trace-element partitioning between amphibole and silicate melt. In *Amphiboles: Crystal Chemistry, Occurrence, and Health Issues*; Hawthorne, F.C., Oberti, R., Della Ventura, G., Mottana, A., Eds.; Mineralogical Society of America: Chantilly, VA, USA, 2007; pp. 417–452.
130. Kumar, A.; Maiti, S.K. Assessment of potentially toxic heavy metal contamination in agricultural fields, sediment, and water from an abandoned chromite-asbestos mine waste of Roro hill, Chaibasa, India. *Environ. Earth Sci.* **2015**, *74*, 2617–2633. [\[CrossRef\]](#)
131. Holmes, A.; Morgan, A.; Sandalls, F.J. Determination of iron, chromium, cobalt, nickel, and scandium in asbestos by neutron activation analysis. *Am. Ind. Hyg. Assoc. J.* **1971**, *32*, 281–286. [\[CrossRef\]](#) [\[PubMed\]](#)
132. Tashakor, M.; Yaacob, W.Z.W.; Mohamad, H.; Ghani, A.A. Geochemical characteristics of serpentinite soils from Malaysia. *Malays. J. Soil Sci.* **2014**, *18*, 35–49.

133. Punturo, R.; Bloise, A.; Critelli, T.; Catalano, M.; Fazio, E.; Apollaro, C. Environmental implications related to natural asbestos occurrences in the ophiolites of the Gimigliano-Mount Reventino Unit (Calabria, Southern Italy). *Int. J. Environ. Res.* **2015**, *9*, 405–418.
134. Mendez, M.O.; Maier, R.M. Phytoremediation of mine tailings in temperate and arid environments. *Rev. Environ. Sci. Biotechnol.* **2008**, *7*, 47–59. [[CrossRef](#)]
135. Huang, L.; Baumgartl, T.; Mulligan, D. Is rhizosphere remediation sufficient for sustainable revegetation of mine tailings. *Annu. Bot.* **2012**, *110*, 223–238. [[CrossRef](#)]
136. Kumaresan, D.; Cross, A.T.; Moreira-Grez, B.; Kariman, K.; Nevill, P.; Stevens, J.; Allcock, R.J.N.; O'Donnell, A.G.; Dixon, K.W.; Whiteley, A.S. Microbial functional capacity is preserved within engineered soil formulations used in mine site restoration. *Sci. Rep.* **2017**, *7*, 564. [[CrossRef](#)]
137. Schimmer, C. Synergistic Use of Soil Microbes and Plants to Facilitate Rehabilitation on Gold Tailings Materials. Master's Thesis, North-West University, Potchefstroom, South Africa, 2017.
138. Northwatch, Mining Watch Canada and Associates. *The Boreal Below: Mining Issues and Activities in Canada's Boreal Forest*; Mining Watch Canada: Ottawa, ON, Canada, 2008; p. 205.
139. Pentreath, R.J. The Discharge of Waters from Active and Abandoned Mines. In *Mining and its Environmental Impact*; Hester, R.E., Harrison, R.M., Eds.; Royal Society of Chemistry: London, UK, 1994; pp. 121–131.
140. Lamb, D.; Erskine, P.D.; Fletcher, A. Widening gap between expectations and practice in Australian mine site rehabilitation. *Ecol. Manag. Restor.* **2015**, *16*, 186–195. [[CrossRef](#)]
141. Cross, A.T.; Stevens, J.C.; Sadler, R.; Moreira-Grez, B.; Ivanov, D.; Zhong, H.; Dixon, K.W.; Lambers, H. Compromised root development constrains the establishment potential of native plants in unamended alkaline post-mining substrates. *Plant Soil* **2019**, *461*, 163–179. [[CrossRef](#)]

Disclaimer/Publisher's Note: The statements, opinions and data contained in all publications are solely those of the individual author(s) and contributor(s) and not of MDPI and/or the editor(s). MDPI and/or the editor(s) disclaim responsibility for any injury to people or property resulting from any ideas, methods, instructions or products referred to in the content.